Journal of Materials Chemistry C

Accepted Manuscript

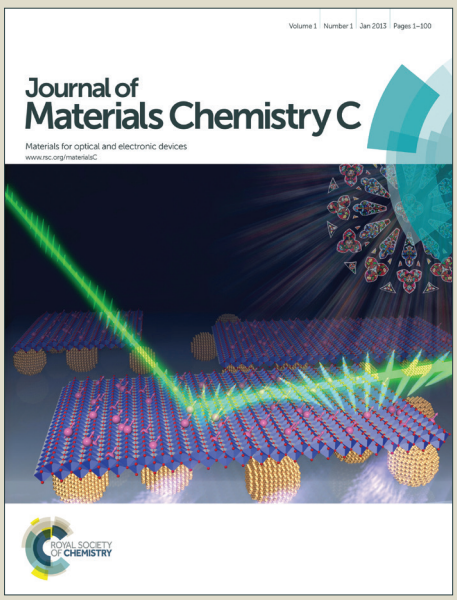

ROYAL SOCIETY OF CHEMISTRY

www.rsc.org/materialsC

Journal Name

RSCPublishing

ARTICLE

Pure and Intense Orange Upconversion Luminescence of Eu^{3+} from the Sensitization of Yb^{3+}-Mn^{2+} Dimer in $NaY(Lu)F_4$ Nanocrystals

Cite this: DOI: 10.1039/x0xx00000x

Received 00th January 2012,
Accepted 00th January 2012

DOI: 10.1039/x0xx00000x

www.rsc.org/

Zhuo Wang,[ab] Jing Feng,[*a] Shuyan Song,[a] Zhiqiang Sun,[c] Shuang Yao,[a] Xin Ge,[a] Min Pang[ab] and Hongjie Zhang[*a]

Pure and intense orange upconversion luminescence of Eu^{3+} was efficiently achieved in $NaYF_4$ and $NaLuF_4$ nanocrystals through upconversion sensitization of doped Yb^{3+} and Mn^{2+} ions dimer for the first time. A shell-coating strategy was performed to further enhance the emission intensity. In this work, a novel upconversion mechanism of energy transfer from Yb^{3+}-Mn^{2+} dimer to Eu^{3+} ion was proposed by analyzing the upconversion luminescence spectra, lifetimes and pumping photons measurements of the obtained nanocrystals in detail. The applications of the nanocrystals for CT imaging and ratiometric pH sensing in physiological pH range were performed. This study also provides a new upconversion spectral region around 592 nm for applications in multicolor imaging, multiplexed encoding and detection.

Introduction

In recent years, lanthanide doped upconversion (UC) luminescent materials which can convert low-energy radiation to high-energy emission through multiphoton processes have attracted extensive interests due to their distinguished merits, including large anti-Stokes shifts, narrow band emissions, long excited-state lifetimes, superior photostability, low cytotoxicity, weak autofluorescence background and deep-tissue penetration.[1-7] These advantages make them extremely suitable in various fields such as solid-state lasers, three-dimensional displays, white light emitting materials, solar cells, temperature sensing, photodynamic therapy, biological labeling and especially optical imaging.[8-17] Up to now, Er^{3+}, Tm^{3+} and Ho^{3+} which have ladder-like arranged energy levels were considered as the most efficient activators among the lanthanide ions due to the facile energy transfer (ET) from the sensitizer Yb^{3+}. However, to achieve efficient upconversion luminescence (UCL) of other lanthanide ions without long-lived intermediary energy states is remain challenging.[18]

Eu^{3+} is well-known for its intense red down-conversion (DC) emission in numerous materials such as coordination compounds, phosphors, nanocrystals (NCs) and lanthanide-containing organic–inorganic hybrid materials.[19-24] Nevertheless, due to the absence of intermediary energy states and large energy mismatch between Yb^{3+} and Eu^{3+}, it is very difficult to achieve efficient UC emission of Eu^{3+} by simply co-doping Yb^{3+} and Eu^{3+} in NCs.[25] Until now, considerable efforts have been devoted to this field and pure UC emission of Eu^{3+} can mainly be obtained by simultaneously harvesting energy of two photons from Yb^{3+} ions *via* cooperative UC processes,[26-31] which is considered weaker and less effective than that of stepwise energy transfer upconversion (ETU) processes in Er^{3+}, Tm^{3+}, Ho^{3+} and Yb^{3+} co-doped systems. Meanwhile, a high-power pump laser is needed for excitation of these materials. This problem greatly restricts the practical applications of Eu^{3+} UCL. To circumvent this issue, several researchers put forward energy migration-mediated upconversion (EMU) mechanism to tune UC processes in core–shell nanoparticles (NPs).[18,32] Albeit relative strong Eu^{3+} UC emissions were attained in these materials, there are also some obvious drawbacks such as the insufficient color purity of Eu^{3+} due to the inevitable contamination of blue light of Tm^{3+} in the core layer and the relatively tedious experimental procedures. Other researchers chose Er^{3+} and Ho^{3+} as sensitizers to excite Eu^{3+}, but the spectral interference from Er^{3+} and Ho^{3+} cannot be eliminated.[33,34]

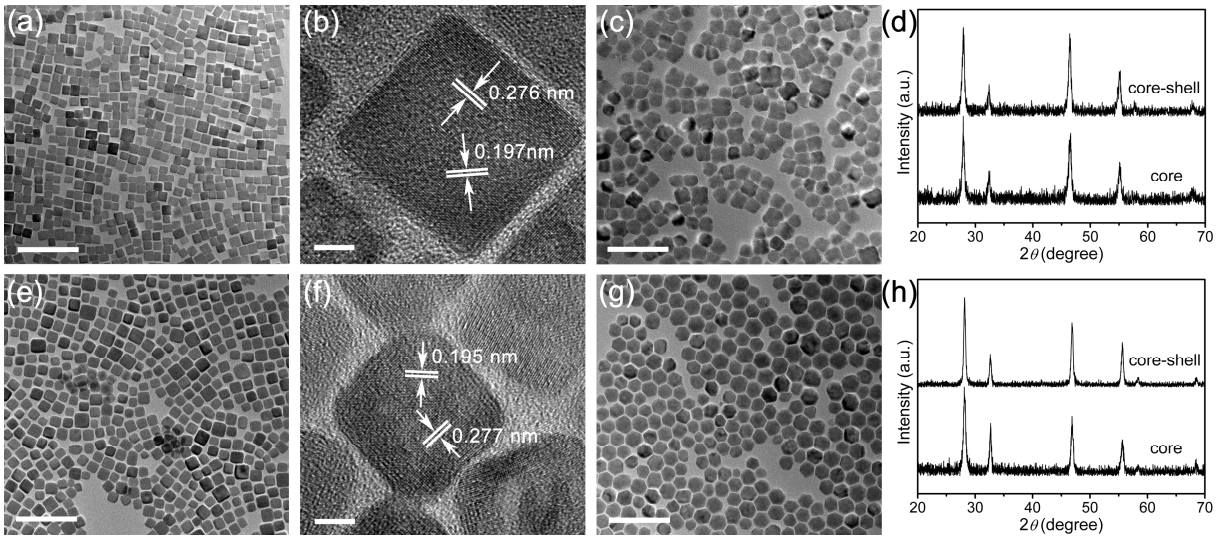

Fig. 1 (a) TEM and (b) HRTEM images of $NaYF_4$:Yb^{3+}/Mn^{2+}/Eu^{3+} (5/30/15 mol%) NCs. (c) TEM image of (a) after $NaYF_4$ shell coating. (d) XRD patterns of (a) and (c). (e) TEM and (f) HRTEM images of $NaLuF_4$:Yb^{3+}/Mn^{2+}/Eu^{3+} (5/30/15 mol%) NCs. (g) TEM image of (e) after $NaLuF_4$ coating. (h) XRD patterns of (e) and (g). The scale bars are 100 nm in (a), (c), (e), (g) and 5 nm in (b), (f), respectively.

In order to overcome these disadvantages, it is necessary to explore a new path to achieve pure and high-efficiency Eu^{3+} UCL. Fortunately, we found that the $^4T_1$ energy level of Mn^{2+} matches very well with the $^5D_0$ energy level of Eu^{3+} and the UCL of Mn^{2+} can be achieved through Yb^{3+}-Mn^{2+} dimer system in various host matrixes.[35-40] In addition, Mn^{2+} is widely used as an energy bridge to get single-band UCL of Er^{3+}, Tm^{3+} and Ho^{3+} in previous work.[41-43] On account of these reasons, we speculate that pure and intense UC emission of Eu^{3+} could be achieved in Yb^{3+}-Mn^{2+}-Eu^{3+} co-doped system. To the best of our knowledge, there is no report focusing on the ET process between Mn^{2+} and Eu^{3+} in UCL materials. As a proof-of-concept experiment to verify the universality of our hypothesis, two frequently-used host lattices $NaYF_4$ and $NaLuF_4$ were chosen as host materials due to their low phonon energy and feasibility for co-doping of Yb^{3+}, Mn^{2+} and Eu^{3+} simultaneously. When Yb^{3+}, Mn^{2+} and Eu^{3+} ions were doped into the hosts, the Yb^{3+}-Mn^{2+} dimers can be easily formed and the energy harvested by Yb^{3+}-Mn^{2+} dimers can be efficiently transferred from the excited state $|^2F_{7/2},^4T_1>$ of Yb^{3+}-Mn^{2+} dimers to the $^5D_0$ energy level of Eu^{3+} ions to generate intense Eu^{3+} UC emission under 980 nm continuous wave laser diode excitation. Meanwhile, the crystalline phase and size of the NCs were greatly influenced by Mn^{2+} doping. To further increase the luminescent intensity, a core-shell structure was designed to minimize surface defects which quench emission intensity of Eu^{3+}. The core-shell NCs which emit intense orange light at around 592 nm can greatly expand the available spectral range of existing UCL materials for applications in multicolor imaging, multiplexed encoding and detection.[44-48] Furthermore, the $NaLuF_4$-based NCs may be ideal multimodal imaging agents for both UC imaging and CT imaging due to strong X-ray absorption of lutetium with the largest atomic number among rare-earth elements.[49-51]

Results and discussion

Synthesis, morphology and phase transformation

The synthesis of $NaYF_4$:Yb^{3+}/Mn^{2+}/Eu^{3+} and $NaLuF_4$:Yb^{3+}/Mn^{2+}/Eu^{3+} NCs was performed employing a modified liquid-solid solution (LSS) solvothermal strategy.[42,52] The epitaxial growth of α-$NaYF_4$ and α-$NaLuF_4$ shell layer on core NCs was conducted according to a previously reported method.[53] Transmission electron microscopy (TEM) images of the obtained NCs before and after the shell growth are shown in Fig. 1. $NaYF_4$:Yb^{3+}/Mn^{2+}/Eu^{3+} (5/30/15 mol%) NCs present cubic in shape and a uniform size of 15.4 nm (Fig. S1a†). The high-resolution TEM (HRTEM) image exhibits well-resolved lattice fringes with a plane spacing of 0.276 nm and 0.197 nm corresponding to the lattice planes of (200) and (220) of α-$NaYF_4$, respectively. After coating of α-$NaYF_4$ shell, the size of the NCs increased to 23.6 nm (Fig. S1b†) indicating the successful epitaxial growth of α-$NaYF_4$ shell layer on core NCs. For $NaLuF_4$:Yb^{3+}/Mn^{2+}/Eu^{3+} (5/30/15 mol%) samples, a number of uniform round-corner cubic NCs with size around 18.9 nm (Fig. S1c†) are clearly observed in the TEM image. In the HRTEM image, the interlayer spacing in a single NC can be precisely measured as 0.277 nm and 0.195 nm, which is in good agreement with the distance between the (200) and (220) planes of α-$NaLuF_4$. After α-$NaLuF_4$ shell coating, the NCs grew up to 24.2 nm (Fig. S1d†), implying that a ca. 3 nm thickness shell was formed on the core. To confirm the chemical composition of the obtained samples, X-ray energy-dispersive (EDX) spectroscopy was used and the results are presented in Fig. S2† which exhibits the presence of pattern peaks of Y, Yb, Mn, Eu and Lu, Yb, Mn, Eu in $NaYF_4$:Yb^{3+}/Mn^{2+}/Eu^{3+} (5/30/15 mol%) NCs and $NaLuF_4$:Yb^{3+}/Mn^{2+}/Eu^{3+} (5/30/15 mol%) NCs, respectively, indicating that the exact ingredients were effectively built into the host lattices.

The powder X-ray diffraction (XRD) patterns of $NaYF_4$:Yb^{3+}/Mn^{2+}/Eu^{3+} (5/30/15 mol%) core and core-shell NCs in Fig. 1d match well with the standard cubic phase $NaYF_4$ (JCPDS: 06-0342), which is consistent with the TEM analysis of the samples. The XRD patterns of $NaLuF_4$:Yb^{3+}/Mn^{2+}/Eu^{3+} (5/30/15 mol%) core and core-shell NCs can be well indexed in accordance with the standard pattern of cubic phase $NaLuF_4$ (JCPDS: 27-0725) as well (Fig. 1h). To understand phase transformation at different Mn^{2+} ,Eu^{3+} and Yb^{3+} doping levels,

XRD patterns of obtained NCs samples with different Mn^{2+} ,Eu^{3+} and Yb^{3+} doping levels are given in Fig. S3-S5†. In the $NaYF_4$:Yb^{3+}/Mn^{2+}/Eu^{3+} (5/y/15 mol%) (y=0-40) serials, the XRD pattern shows a mixed phase of α-$NaYF_4$ (JCPDS: 06-0342) and β-$NaYF_4$ (JCPDS: 16–0334) when no Mn^{2+} ions are added. While the doping concentration of Mn^{2+} ions was increased to 20%, the diffraction peaks of β-$NaYF_4$ completely vanished. Further increasing the Mn^{2+} ions concentration to 40%, the impurity phase of β-$NaYF_4$ reappeared. Meanwhile, the phase transformation is also evident with doping concentration of Eu^{3+}. For $NaYF_4$:Yb^{3+}/Mn^{2+}/Eu^{3+} (5/30/z mol%) (z=0-30) systems, the β-$NaYF_4$ phase appeared when Eu^{3+} concentration was higher than 20%. However, the cubic phase of $NaYF_4$ is relatively stable in the Yb^{3+} doping levels from 2% to 40%. These phenomena are mainly due to the variable ionic radii of the doping ions. The substitution of Y^{3+} (r = 0.89 Å) by smaller Mn^{2+} (r = 0.81 Å) ions tend to produce the cubic phase, while the substitution of larger Eu^{3+} (r = 0.95 Å) ions favors the hexagonal structures. The Yb^{3+} (r = 0.87 Å) ions with ionic radii similar to Y^{3+} ions keep the original phase of $NaYF_4$.[6,42,54,55]

Upconversion luminescent property and energy transfer mechanism

To demonstrate the success of our strategy, UCL spectra of the obtained samples under a 980 nm continuous wave laser diode excitation were recorded, and the results are shown in Fig. 2, together with their optical images. The UCL spectra of both $NaYF_4$:Yb^{3+}/Mn^{2+}/Eu^{3+} (5/30/15 mol%) and $NaLuF_4$:Yb^{3+}/Mn^{2+}/Eu^{3+} (5/30/15 mol%) exhibit characteristic sharp emission peaks of Eu^{3+}, which can be ascribed to the transitions of $^5D_0 \rightarrow {}^7F_1$ (592 nm), $^5D_0 \rightarrow {}^7F_2$ (609 nm), $^5D_0 \rightarrow {}^7F_3$ (650 nm) and $^5D_0 \rightarrow {}^7F_4$ (700 nm) of Eu^{3+}. It is interesting to observe that the transition of $^5D_0 \rightarrow {}^7F_1$ dominants the emission spectra, compared with other peaks. This phenomenon was rarely achieved in Eu^{3+} UC processes, which may be due to the high-symmetry environments around Eu^{3+} ions in α-$NaYF_4$ and α-$NaLuF_4$. It has been well established that the magnetic-dipole transition of $^5D_0 \rightarrow {}^7F_1$ is relatively insensitive to the local symmetry but the electric-dipole transition of $^5D_0 \rightarrow {}^7F_2$ is significantly affected by the symmetry in local environments around Eu^{3+} ions. The transition probability decreases with the increase of symmetry environments around Eu^{3+} ions.[56,57] After inert shell coating, the integrated UCL intensity of these NCs remarkably increased about 9.1 times and 8.4 times for $NaYF_4$:Yb^{3+}/Mn^{2+}/Eu^{3+} (5/30/15 mol%) and $NaLuF_4$:Yb^{3+}/Mn^{2+}/Eu^{3+} (5/30/15 mol%), respectively. Moreover, the full width at half maximum (FWHM) of the $^5D_0 \rightarrow {}^7F_1$ (592 nm) transition was measured to be 9 nm, which is less narrow than the emission peaks in Yb/Er, Yb/Ho and Yb/Tm systems.[41] As shown in Fig. 2, the intense orange luminescence of Eu^{3+} is clearly visible to the naked eyes. To optimize the doping concentration of Mn^{2+}, Eu^{3+} and Yb^{3+}, $NaYF_4$ NCs with different doping levels were prepared (Fig. S6-S8†). We found that the emission intensity of Eu^{3+} dramatically increased with the Mn^{2+} concentration, indicating that Mn^{2+} is a critical ingredient in efficient Eu^{3+} UC in our systems. The optimal Eu^{3+} concentration was determined to be 15 mol%, which is in consistent with the reported work.[18] Different from Er^{3+}, Tm^{3+} and Ho^{3+} UC systems, the optimized concentration of Yb^{3+} was determined to be 5 mol% in our experiments and the UC intensity trends to decrease with the increase of Yb^{3+} content, which may be due to an increased probability of long-distance energy migration that carries excitation energy to lattice or surface defects in high-symmetry unit cells.[58]

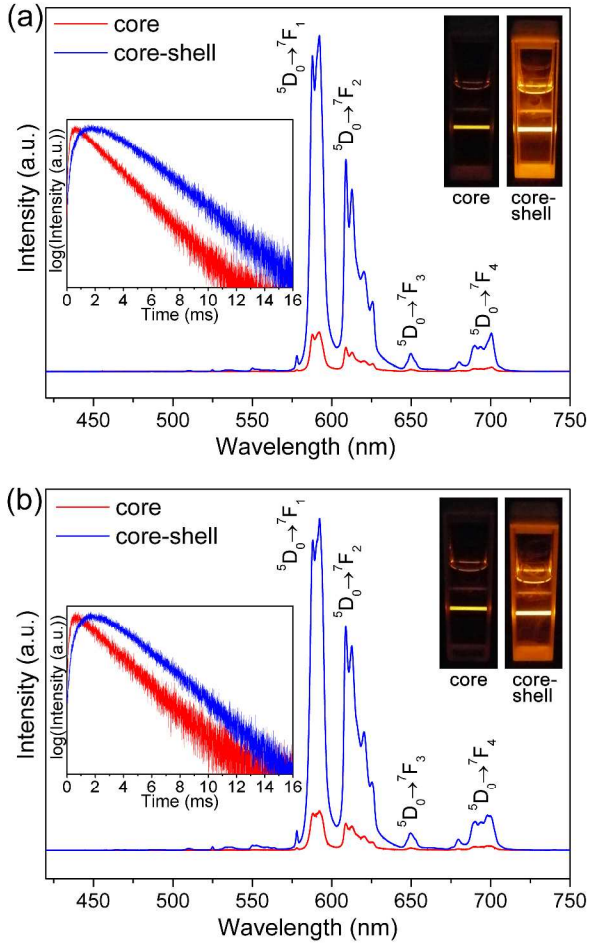

Fig. 2 (a) UCL spectra of $NaYF_4$:Yb^{3+}/Mn^{2+}/Eu^{3+} (5/30/15 mol%) core and core-shell NCs. (b) UCL spectra of $NaLuF_4$:Yb^{3+}/Mn^{2+}/Eu^{3+} (5/30/15 mol%) core and core-shell NCs. Decay curves and luminescence photographs of the corresponding samples in cyclohexane are shown in the left and right insets, respectively. Power density of excitation source is 2.4 W mm^{-2}.

To further validate the effectiveness of core-shell structure on the enhancement of Eu^{3+} UCL and understand the ET processes, the decay curves of the obtained samples were measured at 592 nm emission (Fig. 2). The lifetimes of Eu^{3+} ($^5D_0$) excited states were fitted to be 3.83 ms and 3.99 ms for $NaYF_4$ and $NaLuF_4$ samples, in accordance with single exponential decay process and a notable increase of the Eu^{3+} ($^5D_0$) lifetimes (5.96 ms and 5.63 ms) were observed both in the shell-coated $NaYF_4$ and $NaLuF_4$ samples. Moreover, the rising step of Eu^{3+} emitting level population after the short excitation pulse consumed about 0.6 ms, which is much longer than the excitation pulse, which was considered as a typical feature of an ETU process and very different from the decay curve of cooperative UC process.[59] The cooperative luminescence band of Yb^{3+} was not observed in $NaYF_4$:Yb^{3+}/Mn^{2+}/Eu^{3+} (5/30/15 mol%) or $NaLuF_4$:Yb^{3+}/Mn^{2+}/Eu^{3+} (5/30/15 mol%), which is further confirmed that the cooperative sensitization UC process is very weak in our experiment.[26,31,40] From previous reported

results about an exchange coupled Yb^{3+}-Mn^{2+} dimer model in Mn^{2+} UC,[35-40] it can be deduced that the Yb^{3+}-Mn^{2+} dimer model may also appropriate in $NaYF_4$:Yb^{3+}/Mn^{2+}/Eu^{3+} and $NaLuF_4$:Yb^{3+}/Mn^{2+}/Eu^{3+}. From the crystallographic structure of α-$NaYF_4$ (Fig. S9†), the distance between the nearest Na^+ (Y^{3+}) and Y^{3+} (Na^+) is estimated to be 3.87Å (ICSD 60257) and the Yb^{3+} or Mn^{2+} can substitute the positions of Na^+ or Y^{3+} in α-$NaYF_4$. Hence, the ion couples of Yb^{3+}-Mn^{2+} are close enough to form Yb^{3+}-Mn^{2+} dimers. In $NaYF_4$:Yb^{3+}/Mn^{2+}/Eu^{3+} and $NaLuF_4$:Yb^{3+}/Mn^{2+}/Eu^{3+} NCs, the Yb^{3+}-Mn^{2+} dimer could act as a new kind of sensitizer to harvest energy of two 980 nm photons and transfer to the adjacent Eu^{3+} ion for efficient Eu^{3+} UC emission.

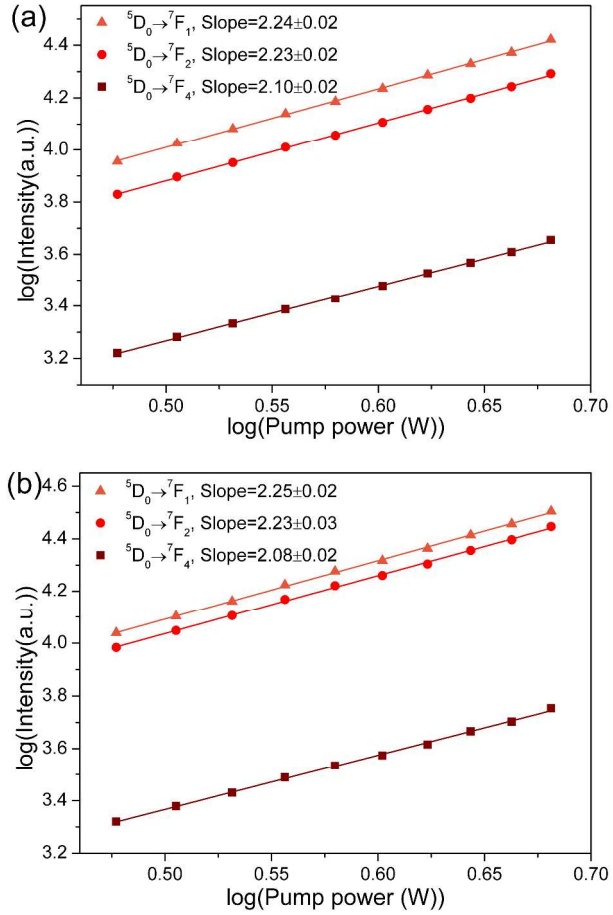

Fig. 3 Pump power dependence of UCL emission intensity of (a) $NaYF_4$:Yb^{3+}/Mn^{2+}/Eu^{3+} (5/30/15 mol%) NCs and (b) $NaLuF_4$:Yb^{3+}/Mn^{2+}/Eu^{3+} (5/30/15 mol%) NCs excited by 980 nm laser.

To gain insight into the UCL mechanism, the study of pump power density dependence on UCL intensity was conducted. In a multiphoton UC process, the dependence of the UCL intensity (I) on the pump power density (P) follows the relation $I \propto P^n$, where the number of pumping photons (n) required to populate the upper state can be determined from the slope of the UCL intensity *versus* the pump power density in a double logarithmic plot.[60] As illustrated in Fig. 3, the fitted slopes of the $^5D_0\rightarrow{}^7F_1$ (592 nm), $^5D_0\rightarrow{}^7F_2$ (609 nm) and $^5D_0\rightarrow{}^7F_4$ (700 nm) emissions for $NaYF_4$ and $NaLuF_4$ samples were determined to be 2.24, 2.23, 2.10 and 2.25, 2.23, 2.08, respectively, indicating a two-photon process involved, which is in good agreement with the population of $^5D_0$ level of Eu^{3+} from the energy transfer of upconverted sensitization of $|^2F_{7/2},{}^4T_1>$ state of Yb^{3+}-Mn^{2+} dimer.

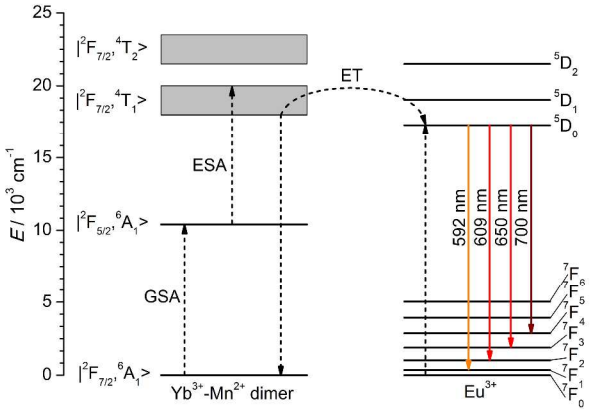

Fig. 4 Proposed energy transfer mechanism in $NaYF_4$:Yb^{3+}/Mn^{2+}/Eu^{3+} NCs and $NaLuF_4$:Yb^{3+}/Mn^{2+}/Eu^{3+} NCs in energy level diagrams of Yb^{3+}-Mn^{2+} dimer and Eu^{3+} ion.

The energy level diagrams of Yb^{3+}-Mn^{2+} dimer and Eu^{3+} ion along with the proposed UC mechanism are shown in Fig. 4. Firstly, the excited state $|^2F_{7/2},{}^4T_1>$ of Yb^{3+}-Mn^{2+} dimer can be populated by sequentially absorbing two 980 nm photons *via* the GSA process ($|^2F_{7/2},{}^6A_1>\rightarrow|^2F_{5/2},{}^6A_1>$) and ESA process ($|^2F_{5/2},{}^6A_1>\rightarrow|^2F_{7/2},{}^4T_1>$). Then, the excited Yb^{3+}-Mn^{2+} dimer drops back to the ground state $|^2F_{7/2},{}^6A_1>$ while transferring the energy to a nearby Eu^{3+} ion to populate the emitting level of $^5D_0$. Finally, the $^5D_0$ level of Eu^{3+} can radiatively decay to $^7F_{1\text{-}4}$ levels to generate intense luminescence at the wavelength of 592 nm, 609 nm, 650 nm and 700 nm, respectively.

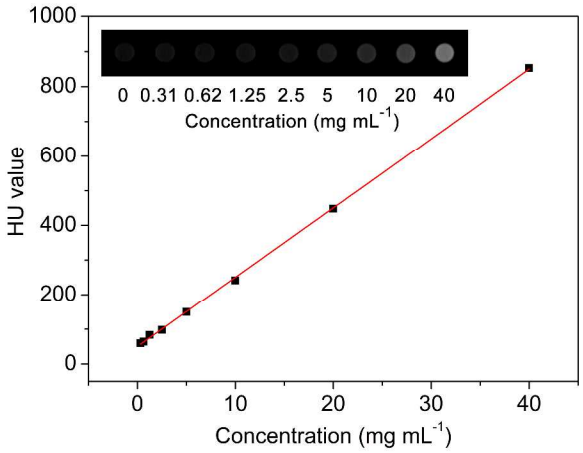

Fig. 5 CT images of aqueous suspension of core-shell $NaLuF_4$:Yb^{3+}/Mn^{2+}/Eu^{3+} NCs with different concentrations and the corresponding HU values.

In vitro CT imaging

For further applications, the oleic acid capped UCNCs (OA-UCNCs) were modified with poly(ethylene glycol)-conjugated phospholipid (DSPE-PEG2000) to yield water soluble PEG-UCNCs. The modified sample was characterized by FT-IR

spectroscopy and two new bands at 1724 cm^{-1} and 1109 cm^{-1} attributed to the stretching vibration of the carboxyl ester and the ether bond of PEG chains appear, indicating the successful surface modification (Fig. S10†).[61] To evaluating the *in vitro* CT imaging property of core-shell $NaLuF_4$:Yb^{3+}/Mn^{2+}/Eu^{3+} NCs, X-ray CT images were acquired using various concentrations of Lu-based PEG-UCNCs dispersed in deionized water (Fig. 5). The CT images became brighter and the measured Hounsfield unit (HU) values of Lu-based PEG-UCNCs increased with the concentrations due to the high X-ray attenuation coefficients of large atomic number rare-earth ions (Lu^{3+}, Yb^{3+} and Eu^{3+}). The *in vitro* CT imaging result is similar to previously reported Lu-based NCs,[49-51] indicating that our material is also a promising CT agent.

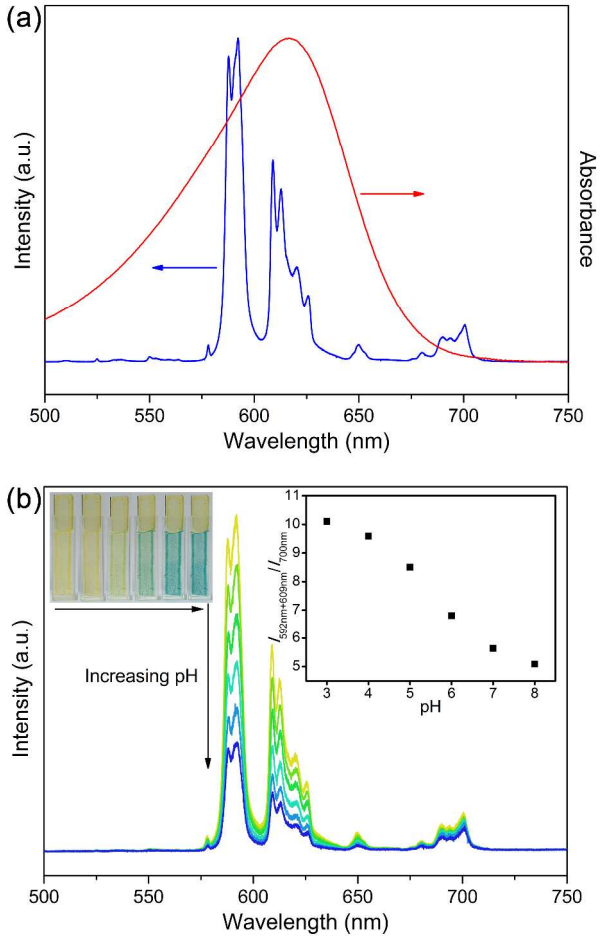

Fig. 6 (a) Absorption spectrum of BCG and BTB mixture (mass ratio=1:1) in buffer solution of pH 8 (red curve) and UCL spectrum of UCNCs (blue curve), (b) UCL spectra and corresponding photographs of the sensor film in buffer solutions of different pH values and the ratio of integrated intensity of $^5D_0 \rightarrow {}^7F_1$ (592 nm) plus $^5D_0 \rightarrow {}^7F_2$ (609 nm) to $^5D_0 \rightarrow {}^7F_4$ (700 nm) at different pH values (inset).

Ratiometric pH sensing

To realize pH sensing in physiological pH range, two commonly-used indicators, bromocresol green (BCG) and bromothymol blue (BTB), were used because the absorption spectra of their base forms perfectly overlap with the $^5D_0 \rightarrow {}^7F_1$ (592 nm) and $^5D_0 \rightarrow {}^7F_2$ (609 nm) UCL emission peaks of the UCNCs (Fig. 6a). From the absorption spectra of BCG and BTB in buffer solutions of different pH values (Fig. S11 and S12†), it can be easily found that the sensitive discoloration ranges are pH 3-6 for BCG and pH 6-8 for BTB, which are in accordance with the pK_a of BCG (4.94) and BTB (6.82), respectively.[62,63] In order to cover the whole physiological pH range, BCG and BTB were mixed together to expand the sensitive discoloration range to pH 3-8 (Fig. S13†). Furthermore, the UCL emission peak of $^5D_0 \rightarrow {}^7F_4$ (700 nm) can be used as an internal reference because it is barely absorbed by the indicators and its intensity keeps constant with the changing of the pH value. The ratiometric pH sensing method based on internal reference also eliminates the interferences caused by the variations of excitation intensity and other measurement conditions. Initial measurements were performed with dispersions of BCG, BTB and $NaYF_4$-based PEG-UCNCs in buffer solutions with different pH values (Fig. S14†). To measure the pH values of flowing samples continuously, BCG, BTB and $NaYF_4$-based PEG-UCNCs were introduced into a sensor film made of a biocompatible polyurethane hydrogel on glass substrate (Fig. 6b). It is obvious that the UCL intensities of both dispersion and sensor film samples decrease with increasing the pH values. The reversibility of the sensor film in buffer solutions with different pH values was investigated as well (Fig. S15†). After several cycles, the response still occurs rapidly between pH 3 and pH 8 within less than 30 s.

Conclusions

In summary, $NaYF_4$:Yb^{3+}/Mn^{2+}/Eu^{3+} and $NaLuF_4$:Yb^{3+}/Mn^{2+}/Eu^{3+} NCs were successfully synthesized by a modified LSS method and intense orange upconversion luminescence of Eu^{3+} was efficiently achieved in the as-prepared materials for the first time. A core-shell strategy was employed to further increase the luminescent intensity. A new energy transfer mechanism of Yb^{3+}-Mn^{2+} dimer to Eu^{3+} ion in Eu^{3+} UC process was proposed according to the exhaustive analysis of the experimental results. The prepared UCNCs were successfully applied in CT imaging and ratiometric pH sensing in physiological pH range as well. The strong UCL emissions of Eu^{3+} endow lanthanide UC materials a novel selective emission at the wavelength around 592 nm for potential applications in multicolor imaging, multiplexed encoding and detection. Furthermore, this new mechanism to achieve intense Eu^{3+} UCL paves a new way for further promoting Eu^{3+} and other lanthanide UC materials.

Experimental section

Materials

$YCl_3 \cdot 6H_2O$ (99.99%), $LuCl_3 \cdot 6H_2O$ (99.99%), $YbCl_3 \cdot 6H_2O$ (99.99%), $EuCl_3 \cdot 6H_2O$ (99.99%), Y_2O_3 (99.99%), Lu_2O_3 (99.99%), CF_3COONa (97%), CF_3COOH (99.0%), oleic acid (OA) (analytical grade), 1-octadecene (ODE) (90%), bromocresol green (BCG) (analytical grade) and bromothymol blue (BTB) (analytical grade) were purchased from Aladdin Reagents. $MnCl_2 \cdot 4H_2O$ (analytical grade) was obtained from Xilong Chemical Co., Ltd. NaOH, NaF, $Na_2HPO_4 \cdot 12H_2O$, citric acid monohydrate, ethanol and cyclohexane were all analytical grade and obtained from Beijing Chemical Reagents. Poly(ethylene glycol)-conjugated phospholipid (DSPE-PEG2000) was purchased from Shanghai Advanced Vehicle Technology Pharmaceutical Ltd. The polyurethane hydrogel D4

was obtained from Cardiotech. All of the reagents and solvents were used as received without further purification. Deionized (DI) water was used throughout. $Y(CF_3COO)_3$ and $Lu(CF_3COO)_3$ were prepared by dissolving Y_2O_3 and Lu_2O_3 in CF_3COOH.

Synthesis of $NaYF_4$:Yb^{3+}/Mn^{2+}/Eu^{3+} NCs

In a typical procedure,[42] a proportionally mixed water solution of YCl_3, $YbCl_3$, $MnCl_2$ and $EuCl_3$ (2 mL, 0.8 mmol of metal ions in total) was added to a mixed clear solution of NaOH (0.24 g), DI water (1.2 mL), ethanol (8 mL) and OA (4 mL) under continuous stirring. Then, 1.6 mL DI water contained 3.2 mmol of NaF was dropwise added to the mixture slowly. After vigorous stirring for 30 min at room temperature, the colloidal solution was transferred into a 20 mL Teflon-lined autoclave, sealed and heated at 200 °C for 8 h. When the autoclave cooled to room temperature naturally, the product was centrifuged and washed with ethanol for several times and then re-dispersed in cyclohexane.

Synthesis of $NaLuF_4$:Yb^{3+}/Mn^{2+}/Eu^{3+} NCs

The $NaLuF_4$:Yb^{3+}/Mn^{2+}/Eu^{3+} NCs were prepared by the same procedure, except for using $LuCl_3 \cdot 6H_2O$ instead of $YCl_3 \cdot 6H_2O$ at the initial stage.

Epitaxial growth of α-$NaYF_4$ shell layer on $NaYF_4$:Yb^{3+}/Mn^{2+}/Eu^{3+} NCs

The epitaxial growth was performed according to a previous method with some modifications.[53] A 0.5 mmol of as-prepared $NaYF_4$:Yb^{3+}/Mn^{2+}/Eu^{3+} (5/30/15 mol%) core NCs, 1 mmol of $Y(CF_3COO)_3$ and 1 mmol of CF_3COONa were added to a mixture of OA (6.5 mL) and ODE (6.5 mL) in a three-necked flask. The mixture was stirred under vacuum to remove oxygen at room temperature for 10 min. Then the mixture was heated to 100 °C with vigorous magnetic stirring in a temperature-controlled electromantle for 30 min to form transparent solution and remove residual water under N_2 flow. The solution was then heated to 250 °C at a heating rate of 20 °C min^{-1} and maintained at this temperature for 30 min under N_2 atmosphere. When the mixture cooled to room temperature, an excess amount of ethanol was added and the product was collected by centrifugation and washed several times with ethanol and then re-dispersed in cyclohexane.

Epitaxial growth of α-$NaLuF_4$ shell layer on $NaLuF_4$:Yb^{3+}/Mn^{2+}/Eu^{3+} NCs

The procedure is similar to epitaxial growth of α-$NaYF_4$ shell layer on $NaYF_4$:Yb^{3+}/Mn^{2+}/Eu^{3+} NCs, except for using $NaLuF_4$:Yb^{3+}/Mn^{2+}/Eu^{3+} (5/30/15 mol%) core NCs and $Lu(CF_3COO)_3$ instead of $NaYF_4$:Yb^{3+}/Mn^{2+}/Eu^{3+} (5/30/15 mol%) core NCs and $Y(CF_3COO)_3$ at the initial stage.

PEG modification of OA-UCNCs

According to a typical method,[42] a chloroform solution (20 mL) containing 200 mg of DSPE-PEG2000 was added to a chloroform dispersion (20 mL) containing 100 mg of core-shell OA-UCNCs with magnetic stirring in a round-bottom flask. The mixture was stirred gently for 12 h. Then chloroform was evaporated using a rotary evaporator on a water bath of 30 °C and the solid was dispersed in DI water under ultrasonication and filtered through 0.22 μm membrane filter. The excess DSPE-PEG2000 was removed by centrifugation.

Sensor film preparation

According to a literature method,[63] BCG (1 mg) and BTB (1 mg) was dissolved in 1.6 g of a solution of 1.0 g of polyurethane hydrogel D4 in 8.1 g of ethanol and 0.9 g of DI water by vigorously stirring. Then, 100 mg of $NaYF_4$-based PEG-UCNCs were added and stirred for 10 h to form a homogeneous mixture. The sensor film was prepared by spreading the mixture onto a glass substrate and drying it at 60 °C.

Characterization

The crystal structures and phase purities of the samples were analyzed by XRD. Measurements were performed on a Bruker D8 ADVANCE X-ray diffractometer with Cu Kα radiation (λ = 1.5418 Å) with an operation voltage and current maintained at 40 kV and 40 mA. TEM and HRTEM images were obtained with a FEI TECNAI G^2 high-resolution transmission electron microscope operating at 200 kV. The UCL spectra were obtained by using a 980 nm laser diode and recorded by a triple grating monochromator (Spectra Pro-2758, Acton Research Corporation). The decay curve measurements were performed and analyzed with a LeCroy WaveRunner 6100 1 GHz oscilloscope. The FT-IR spectra were measured on a Bruker TENSOR 27 FT-IR spectrometer. The absorption spectra were measured on a Shimadzu UV-3600 UV-VIS-NIR spectrophotometer.

***In Vitro* CT imaging**

Various concentrations of Lu-based PEG-UCNCs (40, 20, 10, 5, 2.5, 1.25, 0.62, 0.31 mg mL^{-1}) dispersed in DI water were encapsulated in 1.5 mL plastic tubes and arranged in a line on a plastic shelf. The measurement was conducted using a JL U.A NO.2 HOSP Philips iCT 256 slice scanner with parameters as follows: thickness, 0.9 mm; pitch, 0.99; 120 KVp, 300 mA; field of view, 350 mm; gantry rotation time, 0.5 s; table speed, 158.9 mm s^{-1}.

Sensing of pH

The buffer solutions of different pH values were prepared by dissolving proper amount of $Na_2HPO_4 \cdot 12H_2O$ and citric acid monohydrate in DI water and measured by a digital pH meter (Sartorius PB-10). The absorption spectra of BCG or BTB were measured by adding either 100 μL of BCG ethanol solution (0.5 mg mL^{-1}) or 100 μL BTB ethanol solution (0.5 mg mL^{-1}) into 2 mL of each buffer solution, respectively. The absorption spectra of BCG and BTB mixture were measured by adding both 50 μL of BCG ethanol solution (0.5 mg mL^{-1}) and 50 μL BTB ethanol solution (0.5 mg mL^{-1}) into 2 mL of each buffer solution. The UCL spectra of PEG-UCNCs with BCG and BTB mixture were measured by adding 50 μL of BCG ethanol solution (1 mg mL^{-1}), 50 μL of BTB ethanol solution (1 mg mL^{-1}) and 20 mg of $NaYF_4$-based PEG-UCNCs into 2 mL of each buffer solution. UCL spectra of the sensor film in buffer solutions of different pH values were measured by placing a sensor film in a cuvette containing each buffer solution.

Acknowledgements

The authors are grateful for the financial aid from the National Natural Science Foundation of China (Grant Nos. 21371165, 51372242, 91122030 and 21210001), National Natural Science Foundation for Creative Research Group (Grant No. 21221061), and Jilin Province Youth Foundation (201201008).

Notes and references

[a] State Key Laboratory of Rare Earth Resource Utilization, Changchun Institute of Applied Chemistry, Chinese Academy of Sciences, 5625 Renmin Street, Changchun 130022, China. Email: fengj@ciac.ac.cn, hongjie@ciac.ac.cn
[b] University of Chinese Academy of Sciences, Beijing 100049, China
[c] Cancer Hospital of Jilin Province, Changchun 130021, China

† Electronic Supplementary Information (ESI) available: Supporting Fig. S1–S15. See DOI: 10.1039/b000000x/

1 F. Auzel, *Chem. Rev.*, 2004, **104**, 139-173.
2 F. Wang and X. Liu, *Chem. Soc. Rev.*, 2009, **38**, 976-989.
3 M. Haase and H. Schaefer, *Angew. Chem., Int. Ed.*, 2011, **50**, 5808-5829.
4 H. Dong, L. D. Sun and C. H. Yan, *Nanoscale*, 2013, **5**, 5703-5714.
5 W. Feng, C. Han and F. Li, *Adv. Mater.*, 2013, **25**, 5287-5303.
6 F. Wang, Y. Han, C. S. Lim, Y. Lu, J. Wang, J. Xu, H. Chen, C. Zhang, M. Hong and X. Liu, *Nature*, 2010, **463**, 1061-1065.
7 S. Wang, J. Feng, S. Song and H. Zhang, *CrystEngComm*, 2013, **15**, 7142-7151.
8 T. R. Hinklin, S. C. Rand and R. M. Laine, *Adv. Mater.*, 2008, **20**, 1270-1273.
9 Z. Wang, J. Feng, M. Pang, S. Pan and H. J. Zhang, *Dalton Trans.*, 2013, **42**, 12101-12108.
10 M. Pang, J. Feng, S. Song, Z. Wang and H. J. Zhang, *CrystEngComm*, 2013, **15**, 6901-6904.
11 X. Huang, S. Han, W. Huang and X. Liu, *Chem. Soc. Rev.*, 2013, **42**, 173-201.
12 H. Lian, Z. Hou, M. Shang, D. Geng, Y. Zhang and J. Lin, *Energy*, 2013, **57**, 270-283.
13 F. Vetrone, R. Naccache, A. Zamarron, A. Juarranz de la Fuente, F. Sanz-Rodriguez, L. Martinez Maestro, E. Martin Rodriguez, D. Jaque, J. Garcia Sole and J. A. Capobianco, *ACS Nano*, 2010, **4**, 3254-3258.
14 N. M. Idris, M. K. Gnanasammandhan, J. Zhang, P. C. Ho, R. Mahendran and Y. Zhang, *Nat. Med.*, 2012, **18**, 1580-1585.
15 K. Liu, X. Liu, Q. Zeng, Y. Zhang, L. Tu, T. Liu, X. Kong, Y. Wang, F. Cao, S. A. G. Lambrechts, M. C. G. Aalders and H. Zhang, *ACS Nano*, 2012, **6**, 4054-4062.
16 F. Wang, D. Banerjee, Y. Liu, X. Chen and X. Liu, *Analyst*, 2010, **135**, 1839-1854.
17 J. Zhou, Z. Liu and F. Li, *Chem. Soc. Rev.*, 2012, **41**, 1323-1349.
18 F. Wang, R. Deng, J. Wang, Q. Wang, Y. Han, H. Zhu, X. Chen and X. Liu, *Nat. Mater.*, 2011, **10**, 968-973.
19 C. Yang, L. M. Fu, Y. Wang, J. P. Zhang, W. T. Wong, X. C. Ai, Y. F. Qiao, B. S. Zou and L. L. Gui, *Angew. Chem., Int. Ed.*, 2004, **43**, 5010-5013.
20 A. Huignard, T. Gacoin and J. P. Boilot, *Chem. Mater.*, 2000, **12**, 1090-1094.
21 A. Podhorodecki, M. Banski, A. Noculak, B. Sojka, G. Pawlik and J. Misiewicz, *Nanoscale*, 2013, **5**, 429-436.
22 J. Chen, Q. Meng, P. S. May, M. T. Berry and C. Lin, *J. Phys. Chem. C*, 2013, **117**, 5953-5962.
23 L. D. Carlos, R. A. S. Ferreira, V. d. Z. Bermudez and S. J. L. Ribeiro, *Adv. Mater.*, 2009, **21**, 509-534.
24 J. Feng and H. J. Zhang, *Chem. Soc. Rev.*, 2013, **42**, 387-410.
25 Y. Liu, D. Tu, H. Zhu, R. Li, W. Luo and X. Chen, *Adv. Mater.*, 2010, **22**, 3266-3271.
26 Y. Dwivedi, S. N. Thakur and S. B. Rai, *Appl. Phys. B*, 2007, **89**, 45-51.
27 H. Wang, C. K. Duan and P. A. Tanner, *J. Phys. Chem. C*, 2008, **112**, 16651-16654.
28 I. Hernandez, N. Pathumakanthar, P. B. Wyatt and W. P. Gillin, *Adv. Mater.*, 2010, **22**, 5356-5360.
29 G. Kaur, S. K. Singh and S. B. Rai, *J. Appl. Phys.*, 2010, **107**, 073514.
30 N. Rakov, D. F. Amaral, R. B. Guimaraes and G. S. Maciel, *J. Appl. Phys.*, 2010, **108**, 073501.
31 Y. Dwivedi and S. C. Zilio, *Opt. Express*, 2013, **21**, 4717-4727.
32 Q. Su, S. Han, X. Xie, H. Zhu, H. Chen, C.-K. Chen, R.-S. Liu, X. Chen, F. Wang and X. Liu, *J. Am. Chem. Soc.*, 2012, **134**, 20849-20857.
33 A.-H. Li, Z.-R. Zheng, T.-Q. Lue, Q. Lue and W.-L. Liu, *Opt. Express*, 2009, **17**, 3878-3883.
34 L. Wang, Z. Liu, Z. Chen, D. Zhao, G. Qin and W. Qin, *Opt. Express*, 2011, **19**, 25471-25478.
35 P. Gerner, O. S. Wenger, R. Valiente and H. U. Gudel, *Inorg. Chem.*, 2001, **40**, 4534-4542.
36 C. Reinhard, P. Gerner, R. Valiente, O. S. Wenger and H. U. Gudel, *J. Lumin.*, 2001, **94**, 331-335.
37 C. Reinhard, R. Valiente and H. U. Gudel, *J. Phys. Chem. B*, 2002, **106**, 10051-10057.
38 P. Gerner, C. Fuhrer, C. Reinhard and H. U. Gudel, *J. Alloys Compd.*, 2004, **380**, 39-44.
39 R. Martin-Rodriguez, R. Valiente, F. Rodriguez, F. Piccinelli, A. Speghini and M. Bettinelli, *Phys. Rev. B*, 2010, **82**, 075117.
40 E.-H. Song, S. Ding, M. Wu, S. Ye, F. Xiao, G.-P. Dong and Q.-Y. Zhang, *J. Mater. Chem. C*, 2013, **1**, 4209-4215.
41 J. Wang, F. Wang, C. Wang, Z. Liu and X. Liu, *Angew. Chem., Int. Ed.*, 2011, **50**, 10369-10372.
42 G. Tian, Z. Gu, L. Zhou, W. Yin, X. Liu, L. Yan, S. Jin, W. Ren, G. Xing, S. Li and Y. Zhao, *Adv. Mater.*, 2012, **24**, 1226-1231.
43 Y. Zhang, J. D. Lin, V. Vijayaragavan, K. K. Bhakoo and T. T. Y. Tan, *Chem. Commun.*, 2012, **48**, 10322-10324.
44 O. Ehlert, R. Thomann, M. Darbandi and T. Nann, *ACS Nano*, 2008, **2**, 120-124.
45 L. Cheng, K. Yang, S. Zhang, M. Shao, S. Lee and Z. Liu, *Nano Res.*, 2010, **3**, 722-732.
46 F. Zhang, Q. Shi, Y. Zhang, Y. Shi, K. Ding, D. Zhao and G. D. Stucky, *Adv. Mater.*, 2011, **23**, 3775-3779.
47 H. H. Gorris, R. Ali, S. M. Saleh and O. S. Wolfbeis, *Adv. Mater.*, 2011, **23**, 1652-1655.
48 H. H. Gorris and O. S. Wolfbeis, *Angew. Chem., Int. Ed.*, 2013, **52**, 3584-3600.
49 J. Zhou, X. Zhu, M. Chen, Y. Sun and F. Li, *Biomaterials*, 2012, **33**, 6201-6210.

50 A. Xia, M. Chen, Y. Gao, D. Wu, W. Feng and F. Li, *Biomaterials*, 2012, **33**, 5394-5405.
51 Y. Sun, X. Zhu, J. Peng and F. Li, *ACS Nano*, 2013, **7**, 11290-11300.
52 X. Wang, J. Zhuang, Q. Peng and Y. D. Li, *Nature*, 2005, **437**, 121-124.
53 H. X. Mai, Y. W. Zhang, L. D. Sun and C. H. Yan, *J. Phys. Chem. C*, 2007, **111**, 13721-13729.
54 R. D. Shannon, *Acta Crystallogr., Sect. A: Cryst. Phys., Diffr., Theor. Gen. Crystallogr.*, 1976, **32**, 751-767.
55 D. Chen and Y. Wang, *Nanoscale*, 2013, **5**, 4621-4637.
56 H. X. Mai, Y. W. Zhang, R. Si, Z. G. Yan, L. D. Sun, L. P. You and C. H. Yan, *J. Am. Chem. Soc.*, 2006, **128**, 6426-6436.
57 D. Tu, Y. Liu, H. Zhu, R. Li, L. Liu and X. Chen, *Angew. Chem., Int. Ed.*, 2013, **52**, 1128-1133.
58 J. Wang, R. Deng, M. A. MacDonald, B. Chen, J. Yuan, F. Wang, D. Chi, T. S. A. Hor, P. Zhang, G. Liu, Y. Han and X. Liu, *Nat. Mater.*, 2014, **13**, 157-162.
59 J. F. Suyver, A. Aebischer, D. Biner, P. Gerner, J. Grimm, S. Heer, K. W. Kramer, C. Reinhard and H. U. Gudel, *Optical Materials*, 2005, **27**, 1111-1130.
60 M. Pollnau, D. R. Gamelin, S. R. Luthi, H. U. Gudel and M. P. Hehlen, *Phys. Rev. B*, 2000, **61**, 3337-3346.
61 Y. Liu, K. Ai, J. Liu, Q. Yuan, Y. He and L. Lu, *Angew. Chem., Int. Ed.*, 2012, **51**, 1437-1442.
62 F. Ismail, C. Malins and N. J. Goddard, *Analyst*, 2002, **127**, 253-257.
63 L. N. Sun, H. Peng, M. I. J. Stich, D. Achatz and O. S. Wolfbeis, *Chem. Commun.*, 2009, 5000-5002.

Pure and Intense Orange Upconversion Luminescence of Eu^{3+} from the Sensitization of Yb^{3+}-Mn^{2+} Dimer in $NaY(Lu)F_4$ Nanocrystals

Zhuo Wang,[ab] Jing Feng,[*a] Shuyan Song,[a] Zhiqiang Sun,[c] Shuang Yao,[a] Xin Ge,[a] Min Pang[ab] and Hongjie Zhang[*a]

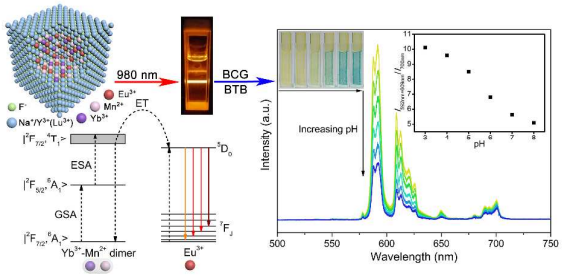

Pure and intense orange upconversion luminescence of Eu^{3+} was efficiently achieved in $NaY(Lu)F_4$ nanocrystals through Yb^{3+}-Mn^{2+} dimer sensitization.